JOURNAL OF MAGNETIC RESONANCE **131,** 209–217 (1998)
ARTICLE NO. MN981360

# Complete Dipolar Decoupling of $^{13}C$ and Its Use in Two-Dimensional Double-Quantum Solid-State NMR for Determining Polymer Conformations

K. Schmidt-Rohr

*Department of Polymer Science & Engineering and Materials Research Science & Engineering Center, University of Massachusetts, Amherst, Massachusetts 01003*

Received October 1, 1997; revised December 2, 1997

**A multiple-pulse technique for complete dipolar decoupling of directly bonded $^{13}C$-labeled sites is described. It achieves significant spectral simplifications in a recently introduced two-dimensional double-quantum solid-state NMR experiment for determining torsion angles. Both homonuclear and heteronuclear dipolar couplings are removed by combining a $^{13}C$ multiple-pulse sequence with continuous-wave irradiation on the protons. The $^{13}C$ sequence has a fundamental 10-pulse cycle which is a significantly modified magic-sandwich-echo sequence. The crucial heteronuclear decoupling is achieved by breaking the 360° ''inner'' pulses in the magic sandwich into 90° pulses and spacing them by $^{1}H$ 360° pulse lengths. Spectral artifacts typical of multiple-pulse sequences are eliminated by phase shifts between cycles. In contrast to many other multiple-pulse decoupling sequences, the long window in the cycle is the dwell time and can be longer than the inverse dipolar coupling, which makes the sequence practical for direct detection even with long pulse ring-down times. A modification of the sequence to scale the chemical shift and increase the effective spectral width is also presented. The 1D and double-quantum 2D experiments are demonstrated on polyethylene with 4% $^{13}C-^{13}C$ spin pairs. The potential of this approach for distinguishing segmental conformations is illustrated by spectral simulations of the two-dimensional ridge patterns that correlate double-quantum and single-quantum chemical-shift anisotropies.** 

*Key Words:* **polymer conformation; magic-sandwich echo; multiple-pulse decoupling; double-quantum NMR; torsion angles.**

## INTRODUCTION

Double-quantum solid-state NMR (*1–7*) on molecules labeled with directly bonded $^{13}C$ spin pairs provides a new and promising approach for determining polymer and peptide structures (*5–7*). In experiments without sample rotation, two-dimensional powder patterns are obtained that reflect the relative orientation of the two $^{13}C$ chemical-shift tensors and thus determine the torsion angle about the intervening bond (*5*). The first, double-quantum, dimension is free of dipolar splittings (*5, 8*) and directly reflects the torsion angle. However, in the original version of the experiment, the directly detected dimension still exhibits $^{13}C-^{13}C$ dipolar splittings, which produce complex spectral patterns, particularly in the intermediate-coupling limit (*5, 9*). The utmost simplification of such two-dimensional patterns is desirable, especially for the analysis of torsion-angle distributions as encountered in amorphous polymers and other disordered solids. The required combination of high-power heteronuclear and homonuclear decoupling during the detection period cannot be achieved by the conventional multiple-pulse sequences for homonuclear decoupling (*10*), such as WHH-4 (*11*), MREV-8 (*12*), or BR-24 (*13*), since the pulses on the S spins reintroduce the I–S dipolar couplings. In addition, for $^{13}C$ detection the sequence must provide particularly long windows before the detection of each point, because the ring-down time of the probe in $^{13}C$ NMR is longer than that in $^{1}H$ NMR.

In this paper, we present a novel $^{13}C$ multiple-pulse sequence combined with high-power proton decoupling that achieves these goals. The $^{13}C$ sequence is derived from the magic-sandwich-echo sequence originally introduced for $^{1}H$ NMR (*14*). It is combined with high-power $^{1}H$ irradiation which removes the heteronuclear dipolar coupling during extra windows introduced into the $^{13}C$ sequence. This produces a sequence with a simple 10-pulse cycle, with a window before data sampling that can be long compared to the inverse of the dipolar couplings. We demonstrate the sequence first in one-dimensional spectra and include a modification that increases the effective spectral width by scaling the chemical shift. Then it is applied during the detection period of the two-dimensional (2D) double-quantum experiment (*5*), in order to obtain clear double-quantum/single-quantum chemical-shift correlation spectra. The resulting two-dimensional patterns are shown to be closely related to hypothetical 2D exchange spectra with full decoupling, but are free of the undesired diagonal ridge. We demonstrate the experiments on polyethylene with dilute (~4%) $^{13}C-^{13}C$ spin pairs. The potential of this approach for distinguishing segmental conformations is illustrated by spectral simulations.



1090-7807/98 $25.00

## THEORETICAL BACKGROUND

Before discussing the new pulse sequence, we briefly review commonly used homo- and heteronuclear decoupling sequences. Results of simple (first-order) average-Hamiltonian theory (*10, 11, 15*), with averaging in the frame toggling with the pulses (*10, 15*), are used to describe the effects of the pulse sequences.

*$^{13}$C homonuclear decoupling.* In $^{1}$H NMR of solids, homonuclear dipolar decoupling is achieved by multiple-pulse sequences such as WHH-4 (*11*), MREV-8 (*12*), or BR-24 (*13*). However, they have several disadvantages which prohibit their application to $^{13}$C sites with directly bonded protons. The NMR signal is detected point by point in the long windows of the sequence, which, however, make up only 40 to 60% of the scaled cycle time. This poses serious problems. On the one hand, the window before the detection must be longer than the pulse ring-down time. On the other hand, making the window long reduces the decoupling efficiency and, more importantly, the effective spectral range, which is equal to the inverse of the scaled cycle time. The useful spectral width is often even further reduced by a factor of 2 due to zero-frequency and imperfect quadrature artifacts. For $^{13}$C detection, the restrictions on the window length are practically prohibitive, since the ring-down time $\tau_r$ for a given quality factor $Q = \omega_0/\Delta\omega_{\text{probe}} = \omega_0\tau_r$ is proportional to $1/\omega_0$, i.e., four times longer for $^{13}$C than for protons at the same field strength. When comparing at equal Larmor frequency, it must be taken into account that the $^{13}$C signal in natural abundance is by a factor of $>100$, and in the slightly $^{13}$C-enriched sample used here by a factor of $\sim 40$, weaker than the corresponding proton signal. The $^{13}$C dead time is longer because the residual $B_1$ field must be reduced to a 40–100 times smaller value than for protons before the $^{13}$C signal can be detected.

A decoupling sequence in which the window before data sampling can be made long and makes up 100% of the scaled cycle time can be produced from magic-sandwich-echo (MSE) cycles, which were developed by Rhim *et al.* (*14*) and utilized in ($^{1}$H) solid-state NMR imaging (*16*). The basic pulse cycle is shown in Fig. 1a. Similar to a spin-lock field, the $n\cdot 360°$ $x$ and $n\cdot 360°$ $(-x)$ pulses average out the chemical shift and produce an average Hamiltonian of $-\frac{1}{2}H_{xx}$, which is transformed into $-\frac{1}{2}H_{zz}$ by the flanking pair of $y\cdots -y$ 90° pulses (*10, 15*). We refer to these two 90° pulses as ''outer'' pulses, and to the intervening pulses in the sandwich as ''inner'' pulses; see Fig. 1a. The phase of the second inner pulse is inverted with respect to the first to eliminate effects of radiofrequency field inhomogeneity. The propagators of the $2n\cdot 360°$ pulses with overall duration $2\tau$ cancel with the propagator for the subsequent period $\tau$ without $^{13}$C pulses,

$$e^{-iH_{zz}\tau}e^{-i(-1/2H_{zz})2\tau} = 1, \qquad [1]$$

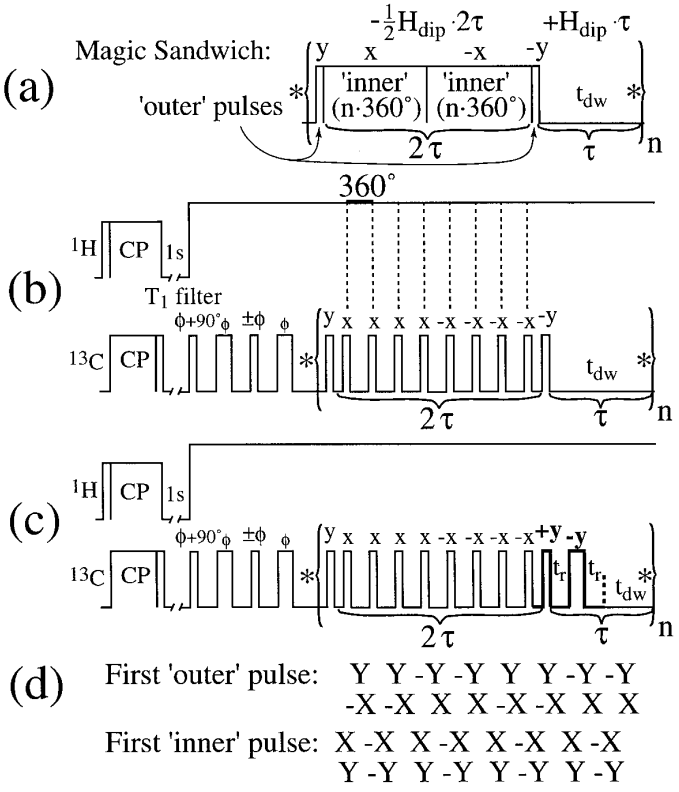


**FIG. 1.** Multiple-pulse sequences providing homonuclear decoupling in $^{13}$C NMR experiments. The points in time where data are sampled are indicated by *. (a) Multiple-pulse sequence based on the magic-sandwich echo, Ref. (*12*), providing homonuclear but no heteronuclear decoupling. (b) Improved 10-pulse cycle, derived from that shown in (a) by splitting the ''inner'' pulses into 90° pulses whose spacings correspond to $^{1}$H 360° pulses. Combined with high-power $^{1}$H irradiation, this provides both homonuclear and heteronuclear decoupling. (c) Chemical-shift scaling introduced into the cycle in (b) in order to increase the effective spectral width. In the pulse sequences (b) and (c) it is shown that before detection, we use a combination of two Hahn echoes with a solid echo, to avoid dead-time problems. (d) Phase cycle used for the first outer and first inner pulse of the 10-pulse sequence in (b). As indicated there, the opposite (negative) phases are used in the corresponding second outer pulse, and in the fifth through eighth inner pulses. Note that the phases are incremented after each 10-pulse block, so that they run through the whole phase cycle several times in each scan. Note also that although the four-pulse blocks are repetitive, leaving parts of them out would result in a different pulse sequence (though only with slightly different properties). The $^{13}$C $T_1$ filter after cross-polarization is specific to our experiments on polyethylene. We suppress the complex signal from the mobile amorphous regions, which have a short $^{13}$C $T_1$ relaxation time, to observe the clear *trans* pattern of the crystalline regions selectively.

and the homonuclear dipolar coupling effects are removed. The signal is sampled conveniently near the end of the window. Since no approximation of short $\tau$ was made, the window need not be short compared to the inverse of the dipolar coupling. The chemical shift is fully effective during the window $\tau$, and averaged out during the inner pulses. Thus, the chemical-shift scaling factor of the magic-sandwich-echo sequence is $\tau/(2\tau + \tau) = \frac{1}{3}$.

*Heteronuclear decoupling.* Efficient $^{13}C-^{1}H$ decoupling is crucial for obtaining highly resolved $^{13}C$ spectra. This is especially important for $CH_2$ groups with their double C–H couplings and strong geminal H–H interaction. In the presence of the strong homonuclear proton coupling, 180° $^{1}H$ pulses, which otherwise eliminate the C–H coupling, do not provide satisfactory decoupling if spaced by more than 10 $\mu$s. Rather, windowless (or nearly windowless) irradiation near resonance, either with a fixed phase or alternating phases (*17, 18*), is required for efficient decoupling (''cw decoupling''). Then, the cycle time is the length of a 360° pulse. Within this time, the heteronuclear coupling is averaged to zero, since the I-spin term in the spin part of the Hamiltonian, $I_zS_z$, nutates through 360° when seen from the toggling frame of the I spins, and vanishes on average (*10, 15*).

*Combined homonuclear and heteronuclear decoupling.* There is no established method for combining MREV-8 homonuclear decoupling with high-power heteronuclear decoupling. It is well known that continuous irradiation on the I spins simultaneous with MREV-8 on the S spins does not average out the heteronuclear coupling since the $I_zS_z$ Hamiltonian in the double (I and S) toggling frame is affected by the pulses on both the I and the S spins (*19*). Instead, 180° pulses on the heteronucleus in the long windows of MREV-8 have been proposed and used for decoupling $^{13}C$ from the protons (*19*). However, this approach is suitable only if the heteronucleus is dilute so that its own homonuclear dipolar couplings are small. In our case, the heteronuclei are the protons, which have strong homonuclear interactions.

Like MREV-8, the original MSE multiple-pulse sequence of Fig. 1a cannot simply be combined with high-power $^{1}H$ irradiation to average the heteronuclear dipolar couplings efficiently. However, it can be modified to provide the heteronuclear decoupling, as will be shown in the following.

As mentioned above, to achieve effective heteronuclear decoupling, 360° $^{1}H$ pulses without simultaneous $^{13}C$ pulsing are required. This can be accomplished in the MSE sequence by introducing windows of the duration of a $^{1}H$ 360° pulse into the ''inner'' $^{13}C$ pulses, as shown in Fig. 1b. The $^{13}C-^{13}C$ dipolar decoupling can be preserved by introducing the windows in such a way that the inner pulses are broken up into 90° $^{13}C$ pulses. The average $^{13}C$ chemical shift and homonuclear dipolar Hamiltonians under the inner pulses are the same with and without the windows: the chemical shift vanishes, while the homonuclear dipolar coupling is scaled by $-\frac{1}{2}$. The long window is extended proportionally. Overall, the chemical-shift scaling factor of the pulse sequence is again $\tau/(2\tau + \tau) = \frac{1}{3}$.

In practice, the $^{13}C$ 90° pulses have a finite, nonnegligible duration. The best decoupling is achieved if the beginnings, or equivalently the centers, of the inner $^{13}C$ pulses are spaced by a $^{1}H$ 360° pulse length $t_{360H}$ as indicated in Fig. 1b. This is found by an average-Hamiltonian calculation for the heteronuclear dipolar coupling $H_{IS} = 2\omega_{IS}I_zS_z$ during the four inner $^{13}C$ 90° $x$ pulses, each of duration $t_{90C}$, and the four $^{1}H$ 360° pulses. The $I_z$ and $S_z$ operators nutate in the doubly toggling frame, with the nutation frequencies of $^{1}H$ and $^{13}C$, $\omega_{1H} = \gamma_H B_{1H}$ and $\omega_C = \gamma_C B_{1C}$, respectively. The average Hamiltonian is found to be zero,

$$\begin{aligned}\bar{H}_{IS} = \frac{2\omega_{IS}}{4t_{360H}} \Bigg\{ & \int_0^{t_{90C}} I(t)(S_z\cos\,\omega_{1C}t + S_y\sin\,\omega_{1C}t)\,dt \\ & + S_y \int_{t_{90C}}^{t_{360H}} I(t)\,dt + \int_0^{t_{90C}} I(t) \\ & \times (S_y\cos\,\omega_{1C}t - S_z\sin\,\omega_{1C}t)\,dt \\ & + (-S_z) \int_{t_{90C}}^{t_{360H}} I(t)\,dt + \int_0^{t_{90C}} I(t) \\ & \times (-S_z\cos\,\omega_{1C}t - S_y\sin\,\omega_{1C}t)\,dt \\ & + (-S_y) \int_{t_{90C}}^{t_{360H}} I(t)\,dt + \int_0^{t_{90C}} I(t) \\ & \times (-S_y\cos\,\omega_{1C}t + S_z\sin\,\omega_{1C}t)\,dt \\ & + S_z \int_{t_{90C}}^{t_{360H}} I(t)\,dt \Bigg\} = 0 \end{aligned} \qquad [2]$$

with $I(t) = I_z\cos\,\omega_{1H}t + I_y\sin\,\omega_{1H}t$. All the integrals are small as such, since $t_{90C}$ is short and the integral of $I(t)$ over a full nutation period $t_{360H}$ vanishes. This makes the further averaging of the four pairs of terms valid. The average Hamiltonian finally vanishes exactly due to sign cancellations. This explains why heteronuclear decoupling works very well. It should be noted that according to an incorrect description that simply assumes that cross-polarization takes place while pulses are applied to $^{13}C$ and $^{1}H$ simultaneously, incomplete decoupling, namely scaling of the coupling to $t_{90C}/t_{360H} \approx 25\%$, would be erroneously expected.

The pulses in the magic-sandwich echo can be extensively phase-cycled in the course of the sequence, since there are only two requirements: (i) the $\pm 90°$ phase shift between the outer and inner pulses, and (ii) the 180° shift between the two outer pulses, and between the first and second half of the inner pulses. Figure 1d lists a phase-cycling scheme that removes zero-frequency peaks and other artifacts efficiently. With this 16-step phase cycle, the total cycle of the pulse sequence consists of $16 * 10 = 160$ pulses, in the same sense in which MREV-8, which consists of two phase-cycled four-pulse WHH-4 cycles, has 8 pulses in its cycle.

The practical limits of the multiple-pulse decoupling sequence of Fig. 1b arise from the length of the detection window, which increases with decreasing $^{13}C$ and $^{1}H$ $B_1$ field strengths. First of all, the length of the window limits the spectral width to between 10 and 25 kHz with typical pulse lengths and dead times. Second, in order for the sequence

to work well, the inverse of the window length, which is ca. 20 kHz in our experiments, must be much larger than the chemical-shift difference of the coupled sites. These conditions are usually met for aliphatic ($sp^3$) carbon sites (at 75 Hz/ppm) but not always for systems with labeled $sp^2$ or $sp^1$ sites. Fortunately, the large chemical-shift differences that create difficulties for the full decoupling sequence usually lead to simple weak coupling patterns, and pure chemical-shift spectra can be produced by techniques other than the modified MSE sequence.

*Chemical-shift scaling.* The spectral width sampled by the multiple-pulse sequence of Fig. 1b is the inverse of the duration of the long window. This may not always be sufficient for preventing aliasing of spectral features. When such a problem arises, the effective spectral width can be increased by scaling down the chemical shift. This can be attained in various ways (*20, 21*), for instance, by reversing and rereversing the chemical shift periodically by pairs of 180° pulses separated by a certain delay $t_r$. In our experiment, special care must be taken to combine the scaling with the dipolar decoupling and to minimize the number of extra pulses. Figure 1c shows a pulse sequence that meets these conditions. For the scaling, only one 180° $^{13}$C pulse is added to the sequence. The other one is effectively produced by inverting the sign of the second 90° outer pulse in the cycle, since for these pulses, $(90°{-}x)(180°x) = (90°x)$. The scaling factor is given by $t_{dw}/\tau = (\tau - 2t_r)/\tau$.

*Hahn–solid–Hahn echo.* In order to detect the first points of the time signal of $^{13}$C–$^{13}$C spin pairs undistorted, i.e., without a dead-time problem, an echo needs to be generated at the start of detection. A 180° pulse which refocuses the chemical shift and resonance offset to create a Hahn echo (*22*) is not sufficient for this purpose, since it does not affect the $^{13}$C–$^{13}$C dipolar couplings (*15*); viewed in a frame toggling with the pulses (*15, 19*), the bilinear spin operator terms $I_\alpha^{(m)}I_\alpha^{(n)}$ ($\alpha = x, y, z$) are inverted together by the 180° pulse, leaving the dipolar Hamiltonian invariant. On the other hand, it has been long known that the dipolar couplings can be refocused by a 90° pulse of suitable phase to produce a solid echo (*15, 23*). However, it is important to note that the solid echo is obtained only if the 90° pulse is applied along the direction of the magnetization. Therefore, we refocus the chemical shift and resonance offset by a 180° pulse in the center of the delay before the 90° pulse. Similarly, the chemical shift and offset effect at the time of the solid echo is removed by a 180° pulse in the center of the delay after the 90° pulse. Thus, Hahn echoes are produced at two crucial times in the solid-echo sequence, and we term the sequence of

$$\tau_e\text{–}(180°{\pm}x)\text{–}\tau_e\text{–}(90°{\pm}x)\text{–}\tau_e\text{–}(180°{\pm}x)\text{–}\tau_e\text{–detection},$$

applied to $x$ magnetization, a Hahn–solid–Hahn echo sequence. All combinations of the signs of the pulses produce magnetization of the same phase, so they can be phase-cycled independently. This three-pulse sequence is shown before the start of detection in the pulse diagrams of Figs. 1 and 2.

The solid echo is exact, i.e., it occurs undistorted and with full amplitude (neglecting relaxation) for delays $\tau_e$ of arbitrary duration, only for a very strongly or a weakly coupled isolated $^{13}$C–$^{13}$C spin pair (*5, 15*). In the intermediate coupling case or for more than two coupled spins, various parts of the Hamiltonian do not commute and the exact result becomes complicated. Nevertheless, noncommutation of the Hamiltonians can be ignored in the short-time limit (*15, 19*) defined by $\omega_{cs}\tau_e \ll 2\pi$, where $\omega_{cs}$ is the chemical-shift difference between the coupled sites, and $\omega_{13C-13C}\tau_e \ll 2\pi$, where $\omega_{13C-13C}$ is the dipolar coupling frequency. With $\tau_e = 20\ \mu s = 1/50$ kHz, this condition can be met easily for the strongest $^{13}$C–$^{13}$C dipolar couplings, which do not exceed 8 kHz, and also for most chemical-shift differences. In fact, for very large chemical-shift differences, the weak coupling limit is reached, in which the sequence works well even for long $\tau_e$ values.

*Two-dimensional double-quantum/single-quantum chemical-shift correlation.* Figure 2 shows the pulse sequence for obtaining fully dipolar-decoupled two-dimensional chemical-shift correlation for isolated $^{13}$C–$^{13}$C pairs. The pulse sequence was obtained by attaching the full dipolar decoupling sequence of Fig. 1b to the double-quantum experiment described in Ref. (*5*). As discussed there, the double-quantum portion of the pulse sequence in Fig. 2 is similar to the refocused INADEQUATE sequence (*24, 25*) used for obtaining connectivity information in solution NMR.

In our experiments, the relative orientations of the chemical-shift tensors of two adjacent segments, as shown for polyethylene in Fig. 3, are determined from two-dimensional ridge patterns. The full dipolar decoupling achieved here yields patterns which are as simple as possible, which facilitates the analysis in the presence of a torsion-angle distribution.

The double-quantum evolution modulates the detected signal of a given segment according to

$$s(t_1, t_2) = g^2(\tau_{DQ})\cos[(\omega_a + \omega_b)t_1]f(t_2) \qquad [3]$$

with a positive transfer function $g^2(\tau_{DQ})$ (*8*). In the original DOQSY experiment (*5*), detection under the $^{13}$C chemical shift and $^{13}$C–$^{13}$C dipolar coupling leads to a relatively complex function $f(t_2)$ and complicated 2D spectral patterns. By applying the complete dipolar decoupling pulse sequence during $t_2$, a much simplified signal

$$s(t_1, t_2) = \langle \overline{g^2(\tau_{DQ})}\cos[(\omega_a + \omega_a)t_1] \times (e^{i\omega_a t_2} + e^{i\omega_b t_2})e^{-(3t_1+t_2)/T_2}\rangle \qquad [4]$$

is obtained. The factor of 3 in the last exponent is due to the scaling factor of the decoupling sequence. The angle

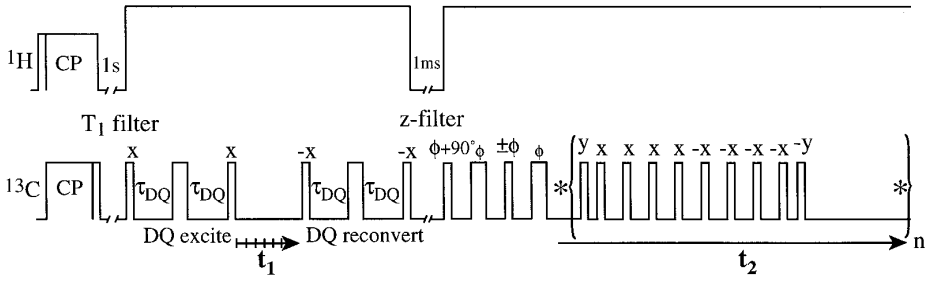


**FIG. 2.** 2D NMR pulse sequence with intrinsically $^{13}C-^{13}C$ dipolar decoupled double-quantum evolution and multiple-pulse decoupled detection according to the sequence of Fig. 1b. The resulting 2D spectrum correlates the sum of the chemical shift in the first dimension with the pure individual chemical shifts. The signal is generated via cross-polarization, the amorphous-phase signal is removed by a $T_1$ filter, the double-quantum coherences are selected by a suitable phase cycle of the reconversion pulses and the receiver phase (*5, 24, 25*), and the dead-time problem is avoided by a 180°–90°–180° pulse Hahn–solid–Hahn echo sequence before detection, as explained in the text.

brackets $\langle\ \ \rangle$ indicate the powder average, while the bar over $g^2(\tau_{DQ})$ indicates the summation of signals for regularly incremented $\tau_{DQ}$ values. If the $\tau_{DQ}$ increment is comparable to the inverse of the $^{13}C-^{13}C$ dipolar coupling constant, and more than about six values are averaged, then

$$\overline{g^2(\tau_{DQ})} \approx \text{const.} \qquad [5]$$

The spectrum $S(\omega_1, \omega_2)$, obtained by double Fourier transformation and taking the real part of the spectrum after suitable phasing,

$$S(\omega_1, \omega_2) = \mathrm{Re}(\mathrm{FT}_{t_1}\{\mathrm{Re}(\mathrm{FT}_{t_2}(s(t_1, t_2)))\}) \qquad [6]$$

can be written as

$$S(\omega_1, \omega_2) = \langle \overline{g^2(\tau_{DQ})}\, 1/2\{A(\omega_1 - (\omega_a + \omega_b)) + A(\omega_1 + (\omega_a + \omega_b))\} \times [A(\omega_2 - \omega_a) + A(\omega_2 - \omega_b)]\rangle \qquad [7]$$

with the absorptive lineshape function $A(\omega)$. The spectrum is measured off resonance so that the signals $A(\omega_1 - (\omega_a + \omega_b))$ and $A(\omega_1 + (\omega_a + \omega_b))$ are located on different sides of $\omega_1 = 0$. Thus, the spectrum of interest, at $\omega_1 > 0$, exhibits peaks at $(\omega_a + \omega_b, \omega_a)$ and $(\omega_a + \omega_b, \omega_b)$. This is the simplest possible peak pattern for a correlation of $\omega_a$ and $\omega_b$, with a single peak per site.

*Relation to 2D exchange spectra.* As mentioned above and discussed in Ref. (*5*), the 2D spectral lineshapes of the double-/single-quantum chemical-shift experiment reflect the torsion angle. In practice, this dependence can be characterized by performing numerical spectral simulations as a function of the torsion angle, which is the only unknown parameter once the chemical-shift tensor orientations have been established by auxiliary experiments. The one-dimensional search for the best fit to the experimental spectrum, e.g., with a series of 36 simulated spectra with 10° $\psi$ increments, can be performed conveniently, provided that all molecules possess the same conformation.

For reading the two-dimensional patterns directly, a more fundamental understanding is desirable. It is achieved by establishing the relation to the corresponding 2D exchange powder patterns (*26–29*), which have been analyzed in considerable detail (*15, 28, 30*). Assuming full dipolar decoupling in both dimensions, which would require application of the full decoupling sequence during both evolution and detection periods, we show in the following that the pure exchange pattern and the DQ/SQ correlation pattern are related by a simple shearing transformation.

For a given segmental orientation, the double-/single-quantum correlation experiment yields spectral lines at $(\omega_a + \omega_b, \omega_b)$ and $(\omega_a + \omega_b, \omega_a)$, while the corresponding exchange signals appear at $(\omega_a, \omega_b)$ and $(\omega_b, \omega_a)$. Thus, the exchange signal at $(\omega_1, \omega_2)$ corresponds to the signal at $(\omega_1 + \omega_2, \omega_2)$ in the double-/single-quantum spectrum. The

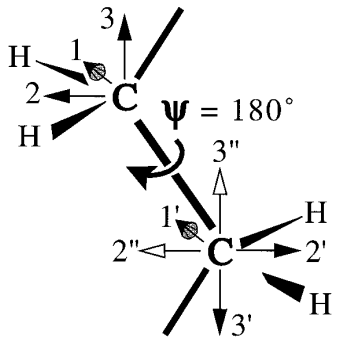


**FIG. 3.** Geometry of two bonded $^{13}C$-labeled $CH_2$ sites in polyethylene crystallites, with their chemical-shift principal-axes systems, from Refs. (*31, 32*), and the intervening torsion angle $\psi$. According to the invariance of the NMR frequency under simultaneous inversion of two of the principal axes [see Ref. (*15*)], the principal-axes systems (1′, 2′, 3′) and (1′, 2″, 3″) are frequency-equivalent. In the *trans* conformation of crystalline polyethylene, as shown in the figure, system (1′, 2″, 3″) is parallel to system (1, 2, 3) of the other site, which means that the chemical-shift frequencies of the two sites are identical.

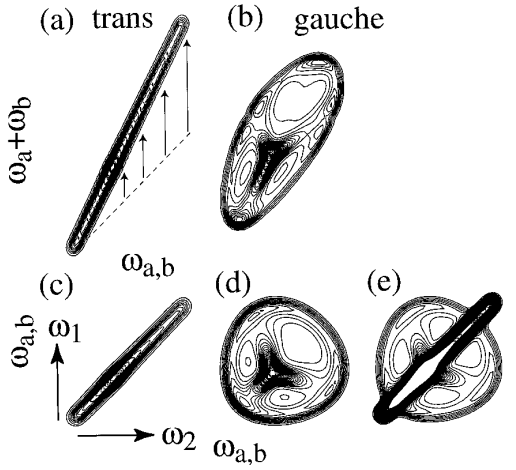


**FIG. 4.** Relation between 2D double-quantum (DQ) spectra (top row) and 2D exchange spectra with full dipolar decoupling (bottom row). The examples shown are calculated with the chemical-shift parameters of polyethylene (*31, 32*). (a) DQ spectrum for a torsion angle $\psi = 180°$ (*trans*). (b) DQ spectrum for $\psi = \pm 60°$ (*gauche*). Spectra for 20 values of $2\tau$, from 140 to 2800 $\mu$s, were coadded. (c) Exchange spectrum for $\psi = 180°$. This pattern is indistinguishable from the diagonal part of the exchange spectrum, which always makes up at least 50% of the integral spectral intensity. (d) Exchange pattern for $\psi = \pm 60°$. (e) Complete exchange spectrum for $\psi = \pm 60°$, including the diagonal ridge, which dominates the spectrum and would mask any contribution of $\psi = 180°$. The contour levels, in 1% increments, range from 2 to 40% of the maximum intensity. Note the similarities between the patterns in (a) and (c), and in (b) and (d). As indicated in (a) by arrows, shearing the exchange pattern by 45° along the $\omega_1$ axis produces the double-quantum pattern.

$\omega_2$-proportional shift in the $\omega_1$ dimension, $(\omega_1, \omega_2) \leftrightarrow (\omega_1 + \omega_2, \omega_2)$, is a definition of the shearing transformation. It moves the diagonal (the line of slope unity) in the exchange spectrum of Fig. 4c onto the line of slope 2 in the double-quantum spectrum of Fig. 4a. (Note that expansion of the $\omega_1$ axis by a factor of 2, which could also make the two mentioned lines coincide, is a different transformation.) Shearing of the exchange pattern for $\psi = \pm 60°$ in Fig. 4d produces the double-quantum pattern of Fig. 4b, apart from a weak modulation by the double-quantum excitation efficiency $g^2(\tau)$.

In the experimental exchange spectra, in addition to the actual exchange patterns of interest here, there is also a strong diagonal ridge resulting from signals at $(\omega_a, \omega_a)$ and $(\omega_b, \omega_b)$. For exchange between the two spins within a $^{13}C-^{13}C$ pair, the diagonal contains at least 50% of the integral intensity. As shown in Fig. 4e, the diagonal ridge is high and dominates the 2D exchange spectrum because it is much less spread out than the exchange signal. Small phase or baseline imperfections of the high diagonal signals can strongly interfere with the exchange patterns.

The signal intensities of the double-quantum and exchange 2D patterns are comparable. In a double-quantum-filtered spectrum, the average signal is smaller than that of the single-quantum spectrum by only a factor of 2 theoretically, and by an overall factor of 3 to 4 experimentally (mostly due to $T_2$ decay during the DQ excitation and reconversion). Since the exchange pattern for a $^{13}C-^{13}C$ spin pair contains only half the intensity, the rest being located on the diagonal, the double-quantum experiment is not inferior in terms of sensitivity. In fact, it has a more favorable dynamic range and fewer artifacts, due to the absence of the overwhelming, uninformative diagonal ridge which dominates the exchange spectrum.

The example of *all-trans*-polyethylene illustrates another advantage of the absence of the diagonal ridge: For an *all-trans* conformation, the tensors of all segments are effectively parallel, as shown for polyethylene in Fig. 3 (*31, 32*). The frequencies are thus all equal, $\omega_a = \omega_b$, and in the 2D exchange spectrum, the exchange signal would coincide with the diagonal and thus not be observable separately. As a result, the *trans–gauche* ratio would be nearly impossible to quantify in a 2D exchange spectrum. In contrast, the double-quantum spectrum shows the *trans* ridge of slope 2, resulting from signals at $(\omega_a + \omega_b, \omega_b) = (2\omega_b, \omega_b)$ and $(\omega_a + \omega_b, \omega_a) = (2\omega_a, \omega_a)$, which proves the *trans* conformation directly.

## RESULTS AND DISCUSSION

Figure 5 displays one-dimensional $^{13}C$ spectra for the crystalline fraction of polyethylene labeled with dilute $^{13}C-^{13}C$ spin pairs. Shown in Fig. 5a is a proton-decoupled cross-

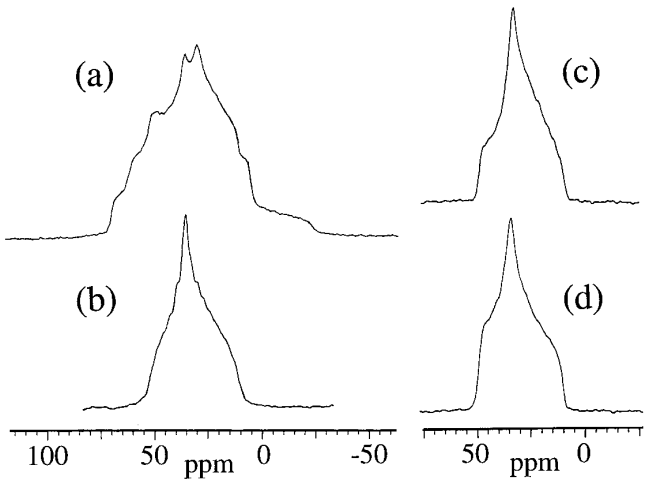


**FIG. 5.** 1D $^{13}C$ powder patterns of the crystalline portion of polyethylene, with $^1H$ decoupling. Spectra of the $^{13}C-^{13}C$-labeled sample (a) without homonuclear decoupling and (b) with homonuclear decoupling using the pulse sequence of Fig. 1b. $^{13}C$ chemical-shift spectra of unlabeled PE for reference: (c) with 63-kHz $^1H$ decoupling and (d) with 80-kHz $^1H$ decoupling. The spectral width in (b) would be twice as large if real and imaginary parts of the signal could be acquired simultaneously (full quadrature detection), as is the case on many modern spectrometers.

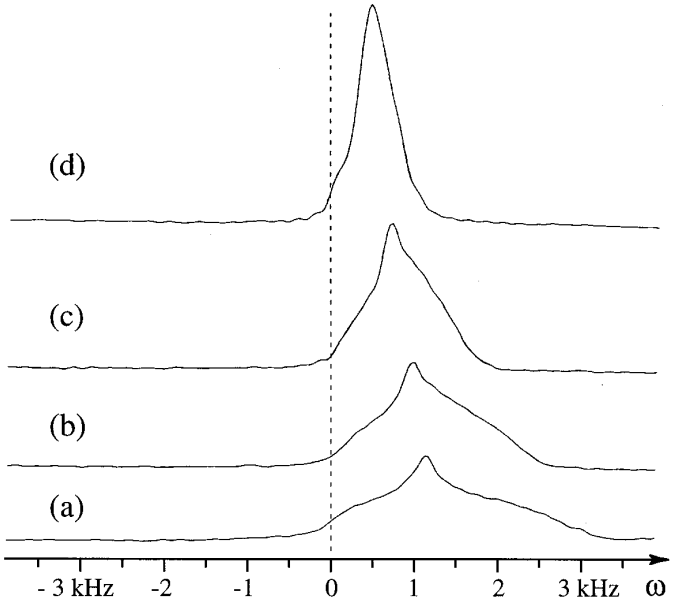


**FIG. 6.** Series of 1D spectra of $^{13}C-^{13}C$-labeled polyethylene with homonuclear decoupling and chemical-shift scaling, using the pulse sequence of Fig. 1c. The carrier frequency is in the middle of the spectral range shown (dashed line). (a) Unscaled, $t_{dw} = \tau = 67\ \mu s$; (b) $t_{dw} = 62\ \mu s$; (c) $t_{dw} = 46\ \mu s$; (d) $t_{dw} = 30\ \mu s$.

polarization spectrum, exhibiting multiple shoulders due to the $^{13}C-^{13}C$ dipolar coupling and ~20% of natural-abundance background signal. A much simpler, regular powder spectrum, Fig. 5b, is obtained by the full dipolar decoupling sequence of Fig. 1b. The spectrum is free of zero-frequency peaks and incomplete-quadrature artifacts that otherwise restrict the useful spectral range in multiple-pulse spectra. The observed lineshape is similar to the $^{13}C$ spectra of unlabeled PE (i.e., without the $^{13}C-^{13}C$ couplings), shown in Fig. 5c and Fig. 5d for different decoupling field strengths.

Figure 6 demonstrates chemical-shift scaling in the fully dipolar-decoupled experiment, using the pulse sequence of Fig. 1c. It shows a series of powder spectra of the labeled PE sample with increasing delay $\tau_r$ and correspondingly decreasing scaling factor. The fixed frequency $\omega = 0$ is located in the center of the spectral range shown. Consequently, in addition to the decrease in the width of the powder pattern, linear shifts of the center of gravity and all features of the spectrum to the center are observed.

The most relevant application of the full decoupling result is a double-quantum/single-quantum chemical-shift correlation experiment on $^{13}C-^{13}C$-labeled molecules, generated by the pulse sequence of Fig. 2. The experimental 2D spectrum obtained for our $^{13}C-^{13}C$-labeled polyethylene sample is displayed in Fig. 7a. It shows a simple pattern consisting of a straight ridge of slope 2 ($\omega_1 = 2\omega_2$). In other words, for all segments $\omega_a + \omega_b = 2\omega_a = 2\omega_b$, and thus $\omega_a = \omega_b$. This proves directly, without requiring a spectral simulation, that the chemical-shift tensors of the two adjacent methylene sites are parallel. This is a characteristic of a *trans* conformation, and consistent with the *all-trans* chain structure in the crystallites of polyethylene. The corresponding simulation for $\psi = 180°$ in Fig. 7b displays the same straight ridge. By contrast, a pattern with an elliptical outline is seen in the simulation for the *gauche* conformation $\psi = \pm 60°$, Fig. 7c. The sensitivity of the spectra to the torsion angle, and the limited overlap of the 2D patterns for *trans* and *gauche* conformations, is apparent. This is a promising starting point for the analysis of the relatively complex torsion-angle distributions expected in amorphous aliphatic polymers.

The main problem with the application of the double-quantum technique to aliphatic sites in disordered systems may be the variability of the chemical shift due to the $\gamma$-*gauche* effect and other conformation-induced factors. In amorphous aliphatic polymers, this leads to significant broadening ($\pm 4$ ppm). To increase the resolution, dipolar couplings can be exploited to separate overlapping patterns. Several applications and extensions of the double-quantum technique are currently being explored in our laboratory.

## CONCLUSIONS

We have presented a solid-state NMR multiple-pulse sequence for measuring chemical-shift spectra of pairs of $^{13}C$-labeled sites, without interference by the $^{13}C-^{13}C$ or $^{13}C-^{1}H$ dipolar couplings. Combined with double-quantum evolution, the new sequence yields very simple and distinctive 2D powder patterns, from which the torsion angle characterizing the conformation of the labeled sites can be determined. The technique introduced here will be the basis of various

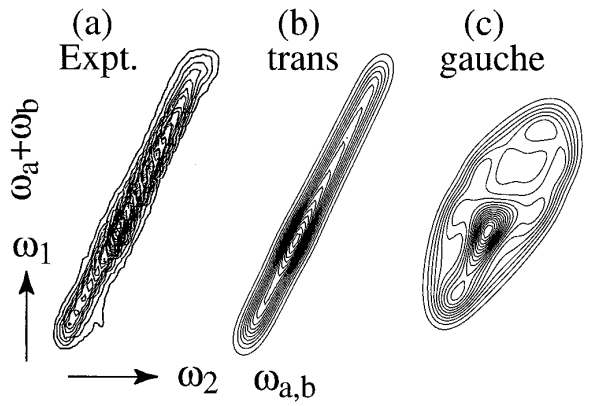


**FIG. 7.** Double-quantum spectrum correlating the sum chemical shift in $\omega_1$ with the pure chemical shifts under multiple-pulse dipolar decoupling in $\omega_2$. (a) Experimental spectrum of the crystalline portion of $^{13}C-^{13}C$-labeled polyethylene, obtained with the pulse sequence of Fig. 2. Signals for eight double-quantum excitation delays, $2\tau = 140, 280, \ldots, 1120\ \mu s$, were coadded. (b) and (c) Corresponding simulations for (b) *trans* and (c) *gauche* ($\psi = \pm 60°$) conformations. The 2D patterns for the two conformations are simple and distinct.

2D and 3D experiments which characterize the segmental structure of amorphous polymers in terms of torsion-angle distributions.

## EXPERIMENTAL

The NMR experiments were performed on a Bruker MSL 300 NMR spectrometer at a $^{13}C$ resonance frequency of 75 MHz. The sample was inserted into the 7-mm coil of a double-resonance Bruker magic-angle-spinning probehead and measured without spinning. The 90° pulse lengths were 4.3 $\mu$s. The proton decoupling field strength during evolution and detection was approximately 80 kHz. A cross-polarization time of 500 $\mu$s and a signal-acquisition time of 7 ms were used.

In all spectra, the signals from the amorphous regions of PE were suppressed by a ''$T_1$ filter,'' where the magnetization generated by cross-polarization is immediately rotated to the $+z$ and $-z$ axes in alternating scans. During the ensuing 1-s delay, the magnetization of the amorphous phase relaxes to the $+z$ direction. Flipping the crystalline-phase magnetization back to its original transverse direction results in the cancellation of the amorphous-phase signal in every other scan. After the $T_1$ filter, the actual pulse sequence is started.

The multiple-pulse chemical-shift detection had a long window and effective dwell time of 56 $\mu$s, and 80 data points were sampled in the time domain. For the 2D experiment, the resonance frequency was set such that the spectrum in the $\omega_1$ dimension was fully off resonance. In the double-quantum dimension, 64 $t_1$ increments were measured. The increment $t_{dw1}$ of the double-quantum evolution time was 28 $\mu$s, such that the spectral width $1/t_{dw1}$ in the $\omega_1$ dimension is four times larger than the double-quantum spectrum. This provides a clean baseplane. To obtain a smooth excitation of the double-quantum coherences for the various dipolar coupling strengths, spectra with eight values of the double-quantum excitation and reconversion delays, $2\tau_{DQ} = 140$, 280, ..., 1120 $\mu$s, were averaged directly during signal acquisition. The measuring time for the 2D spectrum of Fig. 7a was 14 h, or a total of 12,000 scans.

The 2D spectra were processed and plotted on the MSL spectrometer. To obtain pure-phase spectra, the measured ''cosine dataset'' was complemented by slices of zeros in the place of the sine components. Spectral simulations were performed with an angular resolution of 0.25° on a Power Macintosh 8500/120, requiring 30 s per spectrum in a full calculation without approximations.

The doubly labeled polyethylene was prepared by Ziegler–Natta polymerization of a mixture of doubly $^{13}C$-labeled ethene with unlabeled ethene gas.

## ACKNOWLEDGMENTS

Support by NSF/MRSEC is gratefully acknowledged. The author also thanks the Arnold and Mabel Beckman Foundation for support of this work by a Beckman Young Investigator Award. C. Boeffel and H. W. Spiess kindly made the doubly labeled PE sample available. L. C. Dickinson provided excellent hardware support and checked the manuscript. M. Hong provided helpful suggestions on the text. A stimulating discussion with J. D. Gross on the decoupling efficiency was appreciated.

## REFERENCES

1. E. M. Menger, S. Vega, and R. G. Griffin, Double-quantum observation of carbon–carbon dipolar couplings in solids, *J. Magn. Reson.* **56,** 338–342 (1984).
2. R. Tycko and G. Dabbagh, Double-quantum filtering in MAS NMR spectroscopy: An approach to spectral simplification and molecular structure determination, *J. Am. Chem. Soc.* **113,** 9444–9448 (1991).
3. N. C. Nielsen, H. Bildsoe, H. J. Jacobsen, and M. Levitt, Double-quantum homonuclear rotary resonance: Efficient dipolar recovery in MAS NMR, *J. Chem. Phys.* **101,** 1805–1812 (1994).
4. D. M. Gregory, D. J. Mitchell, J. A. Stringer, S. Kiihne, J. C. Shiels, J. Calahan, M. A. Mehta, and G. P. Drobny, Windowless dipolar recoupling: The detection of weak dipolar couplings between spin 1/2 nuclei with large chemical-shift anisotropies, *Chem. Phys. Lett.* **246,** 654–663 (1995).
5. K. Schmidt-Rohr, A double-quantum solid-state NMR technique for determining torsion angles in polymers, *Macromolecules* **29,** 3975–3981 (1996).
6. K. Schmidt-Rohr, Torsion angle determination in solid $^{13}C$-labeled amino acids and peptides by separated-local-field double-quantum NMR, *J. Am. Chem. Soc.* **118,** 7601–7603 (1996).
7. X. Feng, Y. K. Lee, D. Sandström, M. Edén, H. Maisel, A. Sebald, and M. Levitt, Direct determination of a molecular torsional angle by solid-state NMR, *Chem. Phys. Lett.* **257,** 314–320 (1996).
8. T. Nakai and C. A. McDowell, INADEQUATE NMR spectra of extremely strongly coupled spin systems, *Mol. Phys.* **79,** 965–983 (1993).
9. T. Nakai and C. A. McDowell, Characterization of homonuclear spin pairs from 2D spin-echo NMR powder patterns, *J. Am. Chem. Soc.* **116,** 6373–6383 (1994).
10. U. Haeberlen and J. S. Waugh, Coherent averaging effects in magnetic resonance, *Phys. Rev.* **175,** 453–467 (1968); U. Haeberlen, ''High Resolution NMR of Solids,'' Advances in Magnetic Resonance, Supplement 1, Academic Press, San Diego (1976).
11. J. S. Waugh, L. M. Huber, and U. Haeberlen, Approach to high-resolution NMR in solids, *Phys. Rev. Lett.* **20,** 180–182 (1968).
12. W.-K. Rhim, D. D. Elleman, and R. W. Vaughan, Analysis of multiple-pulse NMR in solids, *J. Chem. Phys.* **59,** 3740–3749 (1973).
13. D. P. Burum and W.-K. Rhim, Analysis of multiple pulse NMR in solids. III, *J. Chem. Phys.* **71,** 944–956 (1979).
14. W.-K. Rhim, A. Pines, and J. S. Waugh, Time-reversal experiments in dipolar-coupled spin systems, *Phys. Rev. B* **3,** 684–695 (1971).
15. K. Schmidt-Rohr and H. W. Spiess, ''Multidimensional Solid-State NMR and Polymers,'' Academic Press, London/San Diego (1994).
16. S. Matsui, Y. Ogasawara, and T. Inouye, Proton images of elastomers by solid-state NMR imaging, *J. Magn. Reson. A* **105,** 215–218 (1993).
17. W. A. Anderson and R. Freeman, Influence of a second rf field on high-resolution NMR spectra, *J. Chem. Phys.* **37,** 85–103 (1962).
18. A. E. Bennett, C. M. Rienstra, M. Auger, K. V. Lakshmi, and R. G. Griffin, Heteronuclear decoupling in rotating solids, *J. Chem. Phys.* **103,** 6951–6958 (1995).

*19.* U. Haeberlen, ''High Resolution NMR of Solids,'' Advances in Magnetic Resonance, Supplement 1, p. 86, Academic Press, San Diego (1976).

*20.* J. D. Ellett and J. S. Waugh, Chemical shift concertina, *J. Chem. Phys.* **51,** 2851–2858 (1969).

*21.* W. P. Aue, D. J. Ruben, and R. G. Griffin, Uniform chemical shift scaling: Application to 2D resolved NMR spectra. *J. Chem. Phys.* **80,** 1729–1738 (1985).

*22.* E. L. Hahn, Spin echoes, *Phys. Rev.* **80,** 580–594 (1950).

*23.* J. G. Powles and J. H. Strange, Zero time resolution nuclear magnetic transients in solids, *Proc. Phys. Soc.* **82,** 60 (1963).

*24.* A. Bax, R. Freeman, and S. P. Kempsell, Natural-abundance $^{13}C$–$^{13}C$ coupling observed via double-quantum coherence, *J. Am. Chem. Soc.* **102,** 4849–4851 (1980); A. Bax, R. Freeman, T. Frankiell, and M. H. Levitt, Assignment of $^{13}C$ NMR spectra via double-quantum coherence, *J. Magn. Reson.* **43,** 478–483 (1981).

*25.* R. R. Ernst, G. Bodenhausen, and A. Wokaun, ''Nuclear Magnetic Resonance in One and Two Dimensions,'' Oxford Univ. Press, Oxford (1987).

*26.* H. T. Edzes and J. P. C. Bernards, 2D exchange NMR in static powders: Interchain $^{13}C$ spin exchange in crystalline polyethylene, *J. Am. Chem. Soc.* **106,** 1515–1517 (1984).

*27.* P. H. Henrichs and H. Linder, $^{13}C$ spin diffusion in the determination of intermolecular structure in solids, *J. Magn. Reson.* **58,** 458–461 (1984).

*28.* C. Schmidt, S. Wefing, B. Blümich, and H. W. Spiess, $^{2}H$ 2D exchange NMR in solids, *Chem. Phys. Lett.* **130,** 84–89 (1986).

*29.* G. Dabbagh, D. P. Weliky, and R. Tycko, Determination of monomer conformation in noncrystalline solid polymers by 2D NMR exchange spectectroscopy, *Macromolecules* **27,** 6183–6191 (1994).

*30.* M. Linder, A. Höhener, and R. R. Ernst, Orientation of tensorial interactions determined from 2D NMR powder spectra, *J. Chem. Phys.* **73,** 4959–4970 (1980).

*31.* D. L. VanderHart, Characterization of the methylene $^{13}C$ chemical shift tensor in the normal alkane $n$-$C_{20}$-$H_{42}$, *J. Chem. Phys.* **64,** 830–834 (1976).

*32.* K. Schmidt-Rohr, M. Wilhelm, A. Johansson, and H. W. Spiess, Determination of chemical-shift tensor orientations in methylene groups by separated-local-field NMR, *Magn. Reson. Chem.* **31,** 352–356 (1993).